

Grand canonical diffusion-influenced reactions: a stochastic theory with applications to multiscale reaction-diffusion simulations

Mauricio J. del Razo^{†,a)}, Hong Qian[‡] and Frank Noé^{†,a)}

Abstract: Smoluchowski-type models for diffusion-influenced reactions ($A + B \rightarrow C$) can be formulated within two frameworks: the probabilistic-based approach for a pair A, B of reacting particles; and the concentration-based approach for systems in contact with a bath that generates a concentration gradient of B particles that interact with A . Although these two approaches are mathematically similar, it is not straightforward to establish a precise mathematical relationship between them. Determining this relationship is essential to derive particle-based numerical methods that are quantitatively consistent with bulk concentration dynamics. In this work, we determine the relationship between the two approaches by introducing the grand canonical Smoluchowski master equation (GC-SME), which consists of a continuous-time Markov chain that models an arbitrary number of B particles, each one of them following Smoluchowski's probabilistic dynamics. We show the GC-SME recovers the concentration-based approach by taking either the hydrodynamic or the large copy number limit. In addition, we show the GC-SME provides a clear statistical mechanical interpretation of the concentration-based approach and yields an emergent chemical potential for nonequilibrium, spatially inhomogeneous reaction processes. We further exploit the GC-SME robust framework to accurately derive multiscale/hybrid numerical methods that couple particle-based reaction-diffusion simulations with bulk concentration descriptions, as described in detail through two computational implementations.

[†]Freie Universität Berlin, Department of Mathematics and Computer Science, Arnimallee 6, 14195 Berlin, Germany

[‡]Department of Applied Mathematics, University of Washington, Seattle, WA 98195-3925.

^{a)}Corresponding authors. E-mails: maojrs@gmail.com and frank.noe@fu-berlin.de

I. INTRODUCTION

Smoluchowski's original diffusion-controlled reaction theory describes the bimolecular reaction $A + B \rightarrow C$ in which diffusion is the transport process in solution that determines the encounter between reacting pairs [1, 2]. In such systems, the macroscopic bimolecular reaction rate depends on the diffusion coefficients ($D_A + D_B$). This has been an extremely successful model in physical chemistry [3–9], with current on-going applications [10–20]. The theory assumes that a macromolecule A sits at the origin surrounded by a concentration gradient of B molecules (ligands). If a B molecule gets close enough to A , a reaction occurs and the B is absorbed. This process is mathematically described by a diffusion equation for the concentration gradient of B with an absorbing boundary condition around the A molecule.

A probabilistic version of the same model arose by interpreting Smoluchowski's diffusion equation as a Fokker-Planck equation for one B molecule [3, 8, 11, 21], where the dynamics are now in terms of the *probability density* of finding B at a certain point in space. The two models are mathematically identical except for the far-field boundary condition. The concentration-based approach assumes a constant concentration at infinity, where else the probabilistic approach requires vanishing density at infinity. As there is not yet a clear probabilistic interpre-

tation of the concentration-based approach, the two approaches seem incompatible in a rigorous probability theory. Consequently, there is no theoretical framework to develop probabilistic particle-based simulations that are statistically consistent with bulk concentration dynamics, a highly relevant issue for multiscale/hybrid reaction-diffusion simulations. This brings to light the main key questions addressed in this work:

- What is the connection between Smoluchowski's probabilistic and concentration-based approach?
- Can Smoluchowski's concentration-based approach be interpreted in terms of a probabilistic model?
- How can this connection be employed to develop particle-based simulations that are consistent/coupled with bulk concentration descriptions?

These questions have been partly pointed out before [22] and have been somewhat solved [3, 22, 23]. In the work [3], a microscopic theory (probabilistic) of the kinetics of irreversible (and reversible) diffusion-influenced reactions is developed and extended to pseudo-first-order reactions (very large copy number of B s). In the thermodynamic limit, this theory recovers the law of mass action with the corresponding rate. However, the spatial information is lost and consequently the full connection with Smoluchowski's concentration-based approach too. More recent approaches developed in [14, 24] present a general theory of the kinetics of reversible diffusion-influenced reactions. Unfortunately, it does not reduce to the Smoluchowski's result in the irreversible limit.

On the computational side, [25] offers a good review of previous methods and presents a hybrid approach to couple Brownian dynamics (particle-based) with reaction-diffusion partial differential equations (PDEs) (concentration description). However, it does not generalize to

bimolecular reactions, and it is only presented in one dimension, limiting its applicability. Furthermore, [26] offers an extensive review that discusses the relationship between several particle-based and master equation approaches, which complements many aspects of our work.

In this work, we answer the three questions above by developing a full stochastic theory of diffusion-influenced reactions, called Smoluchowski Master equations (SMEs). Instead of using stochastic diffusion processes in continuous space, SMEs are based on continuous-time Markov chains, where the discrete state space simplifies the calculations and lends itself to computational implementations. Note that, although our work is based on Smoluchowski-type approaches, the results are easily extendable to other diffusion-influenced reaction models, like the Doi model [27], which has certain modeling and simulation advantages [26, 28–30].

We begin Sec. II with an overview of relevant diffusion-influenced reaction models. Based on the probabilistic approach, we derive the first SME for an isolated $A - B$ pair following [11]. In Sec. III, we generalize the SME to an arbitrary nonconstant number of B particles by constructing the grand canonical Smoluchowski Master equation (GC-SME). We further show Smoluchowski's concentration-based approach should be understood as either the hydrodynamic limit (mean-field) or the large copy number limit (law of large numbers) [31, 32] of the GC-SME, a situation analogous to the Kurtz limit [33, 34], where the mass-action ordinary differential equation (ODE) is obtained as the hydrodynamic/large copy number limit of the chemical master equation [35]. This result bridges the probabilistic approach and the concentration-based approach, providing an unequivocal interpretation of Smoluchowski's concentration-based approach in terms of a probabilistic model. It further provides a statistical mechanical interpretation of the concentration-based approach, which elucidates interpretations at the particle level, and it establishes a connection to nonequilibrium thermodynamics through the chemical potential.

Secs. IV and V show how the GC-SME framework can be employed to consistently couple particle-based reaction-diffusion (PBRD) simulations with bulk concentration dynamics in three dimensions. These multi-scale/hybrid schemes have several potential applications, such as: modeling of ion channels [36] and exocytosis [37], where single-particle resolution is fundamental in regions of relevance but unnecessary in the far-field; and modeling of filopodial dynamics [38], where the filopodia is in contact with a larger cytosol compartment that can be modeled in the bulk. These schemes are illustrated through two PBRD simulations that are coupled to material baths: the first one emulates a constant concentration bath, and the second one emulates a time- and space-dependent material bath inspired by the exocytosis process from cell biology. The latter is trivial to generalize to bulk concentration dynamics given in terms of reaction-diffusion PDEs restricted to first-order reac-

tions.

This work is a continuation of [39] into spatiotemporal stochastic chemical kinetics. The previous work provides a general stochastic framework for open nonequilibrium linear networks constructed through Markov chain theory.

II. MODELS OF DIFFUSION-INFLUENCED REACTIONS

In this section, we will review some of the main models of diffusion-influenced reactions; more comprehensive descriptions can be found in [3, 4, 7–9, 27]. Secs. IIA and IIB show an overview of the concentration-based and probabilistic approaches, as well as how they differ from each other. Sec. IIC derives the SME for an isolated pair by discretizing the state space, which will serve as an introduction to the GC-SME from Sec. III.

A. Concentration-based approach

The original diffusion-influenced reactions models for bimolecular reactions $A + B \rightarrow C$ follow a concentration-based approach [1, 2, 6, 40]. In order to derive this model, we assume there is one A represented by a reactive sphere diffusing in space. The frame of reference is fixed at the center of A , and B molecules diffuse freely with a diffusion coefficient given by $D = D_A + D_B$. The concentration gradient of B molecules around A is denoted by $c(r, t)$, and it obeys

$$\frac{\partial c(r, t)}{\partial t} = \nabla \cdot [D \nabla c(r, t)]. \quad (2.1)$$

The concentration in the far-field, $r = R$, is assumed constant, so $c(R, t) = c_0$. The reaction is modeled by a reaction boundary $r = \sigma$ given by the sum of the molecules' radii. Whenever a B molecule reaches σ by diffusion, a reaction occurs immediately. We call this a purely diffusion-controlled reaction since the rate only depends on the time it takes B to diffuse into the reaction boundary. This is modeled with a purely-absorbing boundary condition $c(\sigma, t) = 0$, which yields the steady state and the forward reaction rate

$$c^{ss}(r) = c_0 \left(\frac{R}{R - \sigma} \right) \left[1 - \frac{\sigma}{r} \right], \quad k_S(R) = 4\pi D \sigma \left(\frac{R}{R - \sigma} \right) \quad (2.2)$$

since $k_S(R) = 4\pi D \sigma^2 c^{ss'}(\sigma) / c_0$. As $R \rightarrow \infty$, this simply becomes $c_{\infty}^{ss}(r) = c_0 [1 - \sigma/r]$ and $k_S = 4\pi D \sigma$, which is Smoluchowski's original result [2]. A more general approach uses a partially-absorbing boundary condition [1, 40], $4\pi \sigma^2 D \partial c(r, t) / \partial r|_{r=\sigma} = \kappa c(\sigma, t)$, where κ controls the degree of diffusion influence in the reaction rate. In this case, the steady state and reaction rate as $R \rightarrow \infty$

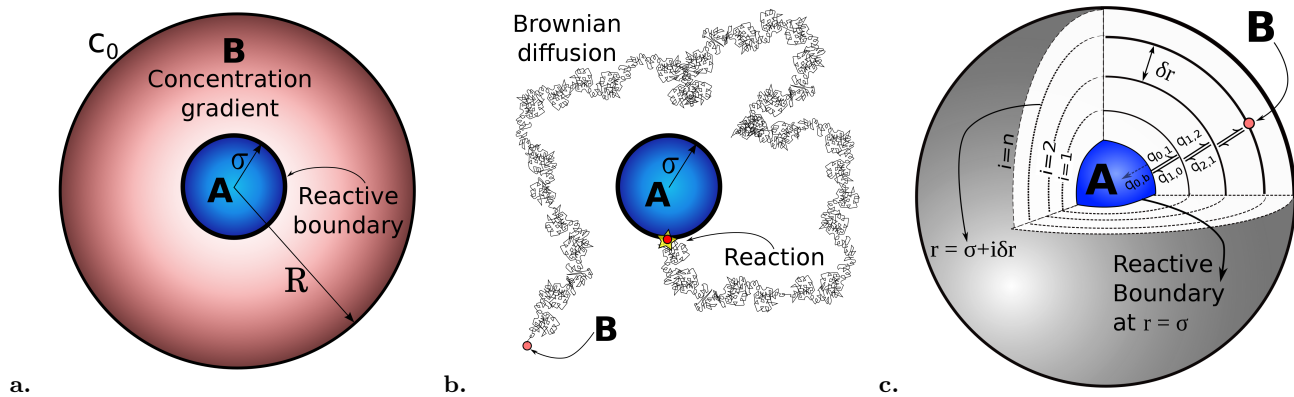


FIG. 1. Illustrations of different models for diffusion-influenced reactions. In the three approaches, A is fixed at the origin and $r = \sigma$ represents the reaction boundary. **a.** The concentration-based approach: A is surrounded by a material bath with concentration c_0 generated by a concentration gradient of B . **b.** The probabilistic approach: one B diffuses around A undergoing Brownian motion. **c.** The SME for an isolated pair: spatial discretization in spherical shells around A of the probabilistic approach. Here we only track on which shell is the B molecule, and the dynamics follow a continuous time Markov chain.

are

$$c^{ss}(r) = c_0 \left[1 - \frac{\kappa\sigma}{k_S + \kappa} \left(\frac{1}{r} \right) \right], \quad k_f = \frac{\kappa k_S}{\kappa + k_S}. \quad (2.3)$$

The purely diffusion-controlled result is recovered as a special case in the limit $\kappa \rightarrow \infty$.

B. Probabilistic approach (for isolated pairs)

If we consider an isolated pair, one A and one B , we can derive a probabilistic theory for diffusion-influenced reactions [3, 8, 21, 41, 42]. Consider A is fixed in the origin and B diffuses following standard Brownian motion. We denote $f(r, t|r_0)$ the probability of molecule B being a distance r from A at time t given that it was at r_0 at time 0. This transition probability will obey the Fokker-Planck equation

$$\frac{\partial f(r, t|r_0)}{\partial t} = \nabla \cdot [D\nabla f(r, t|r_0)], \quad (2.4)$$

$$f(r, 0|r_0) = \frac{\delta(r - r_0)}{4\pi r_0^2}, \quad (2.5)$$

$$4\pi\sigma^2 D \frac{\partial f(r, t|r_0)}{\partial r} \Big|_{r=\sigma} = \kappa f(\sigma, t|r_0), \quad (2.6)$$

$$(2.7)$$

$$\lim_{r \rightarrow \infty} f(r, t|r_0) = 0. \quad (2.8)$$

Eq. (2.5) is the initial condition for the B molecule; Eq. (2.6) models the reaction boundary, and Eq. (2.8) corresponds to vanishing the probability as $r \rightarrow \infty$ due to normalizable total probability. Note this is a well defined stochastic process, where $f(r, t|r_0)$ is the “remaining” probability density function in the presence of an absorbing boundary (diffusion with killing).

Although mathematically similar, the probabilistic approach from Eq. (2.4) seems to be somewhat incompatible with the concentration-based approach from Eq. (2.1). This is due to the difference in the outer boundary condition at $r = R$ (or $r = \infty$) and to dealing with a probability instead of a concentration. In Sec. III, we will understand how these two approaches are related, and the advantages of understanding this relationship.

Note there are alternative models of the reaction process, such as the purely absorbing reaction boundary, $f(\sigma, t|r_0) = 0$, or even a volume reactivity model, like the Doi model [27], which has been recently unified with Smoluchowski-type approaches [8, 43]. Regardless of the reaction process, the main results in Sec. III and the computational schemes from Secs. IV and V remain valid since the results mainly concern the far-field boundary.

C. Smoluchowski master equation

In [11], a discrete time and state Markov chain model for diffusion-influenced reactions for isolated pairs was derived. This model recovers the probabilistic model from Sec. IIB in the continuous space limit. In this section, we will rewrite this model as a Master equation (continuous-time Markov chain).

Consider a macromolecule A fixed at the origin and a ligand B diffusing in the space around it. As we are interested in the diffusive jumps of B in the r direction, we partition the space around A in spherical shells of width δr (Fig. 1c). If the particle is in shell i with radius $r_i = \sigma + i\delta r$, the probabilities to jump to the smaller and bigger shells are $\tilde{q}_{i,i-1}$ and $\tilde{q}_{i,i+1}$, given by $\tilde{q}_{i,i\pm 1} = \delta t (D/\delta r^2 \pm D/(r_{i\pm 1}\delta r))$. This process is a discrete-time Markov chain $\boldsymbol{\pi}^{t+1} = \boldsymbol{\pi}^t \mathbb{P}$, where π_i^t is the probability of B being at spherical shell i at time t , $\boldsymbol{\pi}^t = [\pi_0^t, \pi_1^t, \dots, \pi_i^t, \dots]$, and \mathbb{P} the stochastic matrix in terms of $\tilde{q}_{i,i\pm 1}$. The probability of a reaction $A + B \rightarrow C$

is incorporated into \mathbb{P} by adding $\tilde{q}_{0,b} = \tilde{\kappa}(r)\delta t$, at the innermost shell $r_0 = \sigma$ (reaction boundary)[11]. In order to obtain a Master equation, we can subtract π^t on both sides, divide by δt and take the limit $\delta t \rightarrow 0$ to obtain the SME

$$\frac{d\pi(t)}{dt} = \pi(t)\mathbb{Q}, \quad (2.9)$$

where $\pi(t)$ is the continuous time analog of π^t and the matrix \mathbb{Q} is given by

$$\mathbb{Q} = \begin{bmatrix} -(q_{0,1} + q_{0,b}) & q_{0,1} & 0 & \cdots & \cdots & q_{0,b} \\ \vdots & & \ddots & & & \\ 0 & q_{i,i-1} & -(q_{i,i-1} + q_{i,i+1}) & q_{i,i+1} & & \\ \vdots & & & \ddots & & \end{bmatrix}, \quad (2.10)$$

where the transition rates are given by

$$q_{i,i\pm 1} = \frac{D}{\delta r^2} \pm \frac{D}{r_{i\pm 1}\delta r}, \quad (2.11)$$

and $q_{0,b} = \tilde{\kappa}(r)$. Note the rows of \mathbb{Q} now sum to zero as we should expect from a continuous time Markov chain. The i^{th} equation has the form,

$$\frac{d\pi_i(t)}{dt} = q_{i-1,i}\pi_{i-1}(t) - (q_{i,i-1} + q_{i,i+1})\pi_i(t) + q_{i+1,i}\pi_{i+1}(t). \quad (2.12)$$

Note we are truncating the system up to shell N (the $(N+1)^{\text{th}}$ column of matrix \mathbb{Q}) and that other discretizations are possible [44]. To strictly recover Eq. (2.6), we need $N \rightarrow \infty$. However it is simpler to add $q_{0,b}$ at the end of the first row of the matrix, which corresponds to a periodic boundary condition. This means every time a particle reacts at σ , a new one is placed at the outermost shell r_N . This periodic condition will be consistent with the model from Appendix B; however, it will not be necessary in Sec. III.

This model describes the probability distribution dynamics of one B molecule diffusing around an A molecule with a reaction boundary at σ ; it is the discrete analog of the probabilistic approach from Sec. II B, and it recovers Eq 2.4 in the continuous limit [11]. In the next section, we will construct another discrete-state probabilistic model that is the analog of the concentration-based approach of Sec. II A. The advantage of employing a discrete state space will become evident in Secs. III–V.

III. GRAND CANONICAL SMOLUCHOWSKI MASTER EQUATION

In order to provide a complete probabilistic interpretation of Smoluchowski's original concentration-based approach from Sec. II A, we need to first generalize the SME to an arbitrary number m of B particles in the system. A simple generalization is achieved by assuming the

total number of particles m remains constant (canonical ensemble), see Appendix B. In this section, we present the GC-SME, a generalization of the SME to a nonconstant total number of particles m (grand canonical ensemble). In Sec. III A and Appendix C, we show the GC-SME recovers the concentration-based approach through two different limiting behaviors, resembling Kurtz limit [33, 34], where the mass-action ODE is recovered as a limiting case of the chemical master equation. These results will establish the connection between the probabilistic approach of Sec. II B and the concentration-based approach of Sec. II A. A diagram summarizing the connections between the different models is shown in Fig. 2. In Sec. III B, we provide a statistical mechanical interpretation of the concentration-based model based on the GC-SME in order to clarify interpretations at the particle level. Sec. III C uses the GC-SME to bridge the concept of chemical potential from a probabilistic level to a framework of densities.

We begin with the construction of the GC-SME. Analogous to Sec. II C, we consider a macromolecule A fixed at the origin and partition the space around A in spherical shells of width δr . The dynamics of the B particles are described by a master equation for the joint probability of having n_i B particles in shell i , $P(n_0, n_1, \dots, n_N, t)$, where $\sum_{i=0}^N n_i = m$ is not constant over time. Each particle will diffuse following the SME dynamics, i.e. the rates from Eq. (2.9) and (2.11). The inner boundary is a partially absorbing boundary; however it could be replaced by other reaction processes, like a purely absorbing boundary or a volume reactivity model [27]. The outer boundary allows particles to diffuse out of shell $i = N$ and be annihilated. We further introduce a material bath by adding an additional outer shell $i = N + 1$ with a constant number of particles that can diffuse into shell $i = N$. With these considerations, we can write the GC-SME

$$\begin{aligned} \frac{d}{dt}P(n_0, n_1, \dots, n_N, t) = & \\ \text{reaction boundary} & \left\{ \begin{aligned} & P(n_{0-1}, n_1, \dots, n_N, t)q_{-1,0}(n_{-1}) \\ & + P(n_{0+1}, n_1, \dots, n_N, t)q_{0,-1}(n_0 + 1) \end{aligned} \right. \\ \text{inner diffusion} & \left\{ \begin{aligned} & + P(n_{0+1}, n_{1-1}, \dots, n_N)q_{0,1}(n_0 + 1) \\ & + P(n_{0-1}, n_{1+1}, \dots, n_N)q_{1,0}(n_1 + 1) \\ & + P(n_0, n_{1+1}, n_{2-1}, \dots, n_N)q_{1,2}(n_1 + 1) \\ & + P(n_0, n_{1-1}, n_{2+1}, \dots, n_N)q_{2,1}(n_2 + 1) \\ & \vdots \\ & + P(n_0, \dots, n_{N-1+1}, n_N)q_{N-1,N}(n_{N-1} + 1) \\ & + P(n_0, \dots, n_{N-1-1}, n_N)q_{N,N-1}(n_N + 1) \end{aligned} \right. \\ \text{outer boundary} & \left\{ \begin{aligned} & + P(n_0, \dots, n_{N+1})q_{N,N+1}(n_N + 1) \\ & + P(n_0, \dots, n_{N-1})q_{N+1,N}(n_N + 1) \end{aligned} \right. \\ \text{leaving state} & \left\{ \begin{aligned} & - P(n_0, \dots, n_N) \sum_{k=0}^N [q_{k,k+1} + q_{k,k-1}] n_k. \end{aligned} \right. \end{aligned} \quad (3.13)$$

We divided the terms of the GC-SME into four categories: the incoming transitions to the current state

through the reaction boundary, the incoming transitions to the current state through diffusion of particles in the inner shells, the incoming transitions to the current state through the outer boundary in contact with a material bath and the transitions leaving the current state through diffusion or escape through either of the boundaries.

A. Hydrodynamic limit

In this section, we show the mean-field of the GC-SME recovers the concentration-based approach in the continuous limit (hydrodynamic limit), finalizing a clear-cut connection between the probabilistic and the concentration-based approach (Fig. 2).

We obtain the mean-field of the GC-SME by deriving an equation for the expected number of molecules at shell i . Multiplying the GC-SME by n_i , summing over all the possible number of molecules $\{\bar{n}\} = \{n_0, \dots, n_N\}$ for all $j = 0, 1, 2, \dots$, using that $\langle n_i \rangle = \mathbb{E}[\mathcal{N}_i = n_i]$ and doing some algebra, we obtain the mean-field equation

$$\begin{aligned} \sum_{\{\bar{n}\}} n_i \frac{d}{dt} P(n_0, n_1, \dots, n_N, t) &= \frac{d \langle n_i \rangle}{dt} = \\ &\underbrace{\langle n_{i+1} \rangle q_{i+1,i} - \langle n_i \rangle [q_{i,i+1} + q_{i,i-1}] + \langle n_{i-1} \rangle q_{i-1,i}}_{\text{absorbing boundary} + \text{inner diffusion} + \text{outer boundary}} \\ &\quad + \sum_{j=-1}^N [\langle n_i n_j \rangle q_{j,j+1} + \langle n_i n_{j+1} \rangle q_{j+1,j}] \\ &\underbrace{- \sum_{j=0}^N \langle n_i n_j \rangle [q_{j,j+1} + q_{j,j-1}] - \langle n_i n_{N+1} \rangle q_{N+1,N}}_{\text{leaving state}}. \end{aligned}$$

As $q_{-1,k} = 0$ for all k , and $q_{0,-1} = q_{0,b}$, we can join the two series together. All the terms in the series will cancel out except for one. This remaining term will also cancel out with the second term from the “leaving state”. The only terms left over are

$$\frac{d \langle n_i \rangle}{dt} = \langle n_{i+1} \rangle q_{i+1,i} - \langle n_i \rangle [q_{i,i+1} + q_{i,i-1}] + \langle n_{i-1} \rangle q_{i-1,i}. \quad (3.14)$$

Renaming $F_i(t) = \langle n_i \rangle$, we have exactly the same equation as Eq. (B.3), so we will have the same limiting behavior as the one studied in detail in Appendix B. We will now take the continuous limit. We first substitute the transition rates from Eq. (2.11) to obtain

$$\begin{aligned} \frac{dF_i(t)}{dt} &= D \left[\frac{F_{i+1}(t) - 2F_i(t) + F_{i-1}(t)}{\delta r^2} \right] \\ &\quad - \frac{2D}{r_i} \left[\frac{F_{i+1}(t) - F_{i-1}(t)}{2\delta r} \right] + \frac{D}{\delta r} \left[\frac{F_i(t)}{r_i - \delta r} - \frac{F_i(t)}{r_i + \delta r} \right], \end{aligned} \quad (3.15)$$

which is the same as Eq. (B.4). Taking the limit $\delta r \rightarrow 0$ and scaling the geometrical effects (Eq. (B.6)), we recover

the Smoluchowski equation (Eq. 2.1)

$$\frac{\partial f(r, t)}{\partial t} = \frac{D}{r^2} \frac{\partial}{\partial r} \left(r^2 \frac{\partial f(r, t)}{\partial r} \right),$$

where the function $f(r, t)$ is the expected value for the concentration. However, in this case, the interesting behavior will be at the boundaries ($i = 0, N$ in Eq. (3.14)). The resulting equations are

$$\frac{dF_0(t)}{dt} = -(q_{0,1} + q_{0,b})F_0(t) + q_{1,0}F_1(t), \quad (3.16)$$

$$\begin{aligned} \frac{dF_N(t)}{dt} &= q_{N+1,N}n_{N+1} - (q_{N,N+1} + q_{N,N-1})F_N(t) \\ &\quad + q_{N-1,N}F_{N-1}(t), \end{aligned} \quad (3.17)$$

where we used the fact that the number of particles at $i = N+1$ is fixed, $\langle n_{N+1} \rangle = n_{N+1}$. In the continuous limit, in the same way as Eq. (B.7), the equation for the inner boundary, Eq. (3.16), will yield the boundary condition for the inner absorbing boundary

$$4\pi D \sigma^2 \frac{\partial f(r, t)}{\partial r} \Big|_{r=\sigma} = \kappa f(\sigma, t).$$

In order to determine the boundary condition in the far-field, we apply the same methodology to Eq. (3.17). We introduce a ghost cell at $i = N+1$, \tilde{F}_{N+1} . By adding and subtracting terms with \tilde{F}_{N+1} , we rewrite Eq. (3.17) in such a way that we have all the terms from Eq. (3.15) plus some additional terms. Writing the rates explicitly, we obtain

$$\begin{aligned} \frac{dF_N(t)}{dt} &= D \left[\frac{\tilde{F}_{N+1}(t) - 2F_N(t) + F_{N-1}(t)}{\delta r^2} \right] \\ &\quad + \frac{D}{\delta r} \left[\frac{F_N(t)}{r_N - \delta r} - \frac{F_N(t)}{r_N + \delta r} \right] - \frac{D}{\delta r^2} \tilde{F}_{N+1}(t) + n_{N+1} q_{N+1,N} \\ &\quad + \tilde{F}_{N+1}(t) \frac{D}{r_N \delta r} - \frac{2D}{r_N} \left[\frac{\tilde{F}_{N+1}(t) - F_{N-1}(t)}{2\delta r} \right] \end{aligned}$$

In order to satisfy the main equation (Eq. (3.15)), the additional terms must be zero, so the ghost cell needs to satisfy

$$n_{N+1} q_{N+1,N} = \left[\frac{D}{\delta r^2} - \frac{D}{r_N \delta r} \right] \tilde{F}_{N+1}(t).$$

We apply directly the scaling from Eq. (B.6); however, in this case $F_i(t)$ is still discrete, so $F_i(t) = 4\pi r_i^2 f(r_i, t) \delta r$. Additionally, the concentration c_0 in the outermost shell is given by $c_0 = n_{N+1} / 4\pi r_{N+1}^2 \delta r$. We will also call the rate of incoming particles $\gamma = q_{N+1,N}$. Substituting these into the equation, we obtain

$$\begin{aligned} c_0 4\pi r_{N+1}^2 \delta r \gamma &= \left[\frac{D}{\delta r^2} - \frac{D}{r_N \delta r} \right] 4\pi r_{N+1}^2 \tilde{f}(r_{N+1}, t) \delta r, \\ \Rightarrow c_0 \delta r^2 \gamma &= \left[1 - \frac{\delta r}{r_N} \right] D \tilde{f}(r_{N+1}, t). \end{aligned}$$

In order to obtain a convergent limit, we need to set the transition rate γ to have the value

$$\gamma = \frac{D}{\delta r^2} - \frac{D}{r_N \delta r}, \quad (3.18)$$

which yields $c_0 = \tilde{f}(r_{N+1}, t)$. The limit as $\delta r \rightarrow 0$ yields

$$f(r_{\max}, t) = c_0,$$

where the number of particles n_{N+1} corresponds to a constant bath concentration of c_0 . The rate γ corresponds to the diffusion rate for the corresponding discretization, which is intuitively consistent. Other values of γ could be provided in the discrete model, but they will not produce the correct continuous limit. This result shows the concentration-based approach, with its corresponding boundary conditions, is recovered in the hydrodynamic limit of the GC-SME; it is referred to as hydrodynamic limit following the literature of interacting particle systems [31, 32].

Note there was a hidden assumption when we stated $c_0 = n_{N+1}/4\pi r_{N+1}^2 \delta r$. The state $N+1$ is different to all the others since the number of particles does not change even though the system is continually absorbing particles from it. This is only feasible if it can access an infinite number of particles. When assuming a constant concentration $c_0 = n_{N+1}/4\pi r_{N+1}^2 \delta r$, we actually refer to the concentration of the whole bath

$$c_0 = \frac{3n_{\text{bath}}}{4\pi(R_\infty^3 - r_N^3)}.$$

In order to have access to an infinite amount of particles, we need to make the corresponding volume infinite, $R_\infty \rightarrow \infty$. At the boundary layer of width δr around r_N , the concentration has to be $c_0 = n_{N+1}/4\pi r_{N+1}^2 \delta r$, where $n_{N+1} \rightarrow 0$ as $\delta r \rightarrow 0$. Although it might appear the number of particles of the bath goes to zero, it is actually the opposite; the number of particles and the volume in the bath must go to infinity at a fixed rate.

In addition to the hydrodynamic limit, one can also show that the concentration-based approach is also recovered in the large copy number limit of the GC-SME; this result is shown in Appendix C.

With these results, we finalize the connection between the probabilistic and the concentration-based approach, see Fig. 2. Smoluchowski’s original concentration-based approach is therefore better understood in terms of a probabilistic model in two different ways, as the hydrodynamic limit or as the large copy number limit of the GC-SME. Note the latter does not require taking the mean field. However, it is not surprising these two limits converge to the same result since this is a linear system.

These results will further allow us to generate particle-based simulations that are consistent with concentration descriptions (Secs. IV and V). The results of one of the simulations is shown in Fig. 3, where the two types of convergence of the GC-SME are illustrated with particle-based simulations.

We should also emphasize the relevance of moving into a discrete state setting since it is not clear how one could write the GC-SME using a continuous state spectrum.

B. Statistical mechanical interpretation

We showed that Smoluchowski’s original concentration-based approach emerges from the hydrodynamic/large copy number limit of the GC-SME. This connection yields specific interpretations of Smoluchowski’s original model. In order to elucidate them, first note there are two equivalent interpretations of a system in the grand canonical ensemble [45]:

1. The system is immersed in a large reservoir with which it can exchange energy and particles.

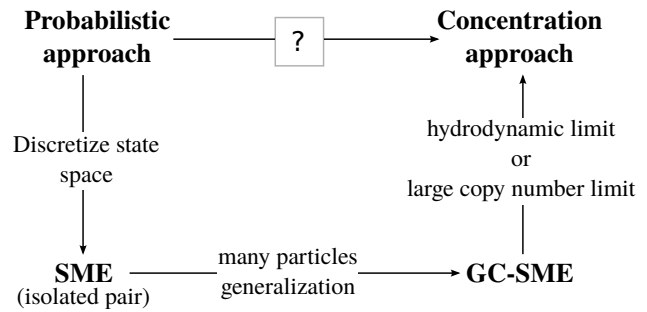


FIG. 2. Diagram showing the relationships between the different models. The initial unknown is how Smoluchowski’s probabilistic and concentration-based approaches relate to each other. In order to resolve this, we first derive the SME, which is a state-space discretization of the probabilistic approach. Then we derive the GC-SME, a stochastic model that generalizes the SME to a large number of B particles (non-constant). Finally, the concentration-based model is recovered as the hydrodynamic limit (mean-field) or large copy number limit of the GC-SME. As in particle-based simulations, one requires to know the dynamics of the stochastic trajectories, this connection allows developing particle-based simulations that are consistent with bulk concentration dynamics.

2. The given system and a large number of “hypothetical copies” can exchange energy and particles with each other.

Smoluchowski’s concentration-based approach is framed following 1; there is one macromolecule A in the origin surrounded by a concentration gradient of B ligands. A acts as a sink of ligands since it can react with an infinite number of them. In most realistic settings, a macromolecule can only react with one or a finite number of ligands, so why Smoluchowski’s original approach models so many systems successfully? If we concentrate on the GC-SME instead of the original concentration approach, given that B particles are treated as independent entities, we can easily frame the model following either interpretation 1 or 2. The GC-SME therefore allows us to interpret Smoluchowski’s concentration-based approach following 2: consider an ensemble of systems each with one macromolecule A and all inside some solution. Each system in our ensemble corresponds to a small neighborhood around each A , where there are no other A ’s. The B ligands in the solution are plentiful and can diffuse through the whole solution. Therefore, they can be exchanged between the different systems of our ensemble. This description does not require one A to react with a large number of B ’s because our ensemble has a large number of A ’s as well. This means that the concentration gradient resulting from Smoluchowski’s original theory is the average concentration we would observe when looking around each one of the A ’s in the solution.

Although this interpretation was previously stated in [3, 7], the GC-SME further provides a precise probabilistic interpretation, enabling explicit implementation of particle exchange mechanisms that are consistent with concentration-based models. It should be pointed out that different exchange mechanisms at the particle level could potentially yield the same mean-field behavior; however, physical arguments on a case by case basis can be used to discard alternative mechanisms. In our case, the particles are injected into the system

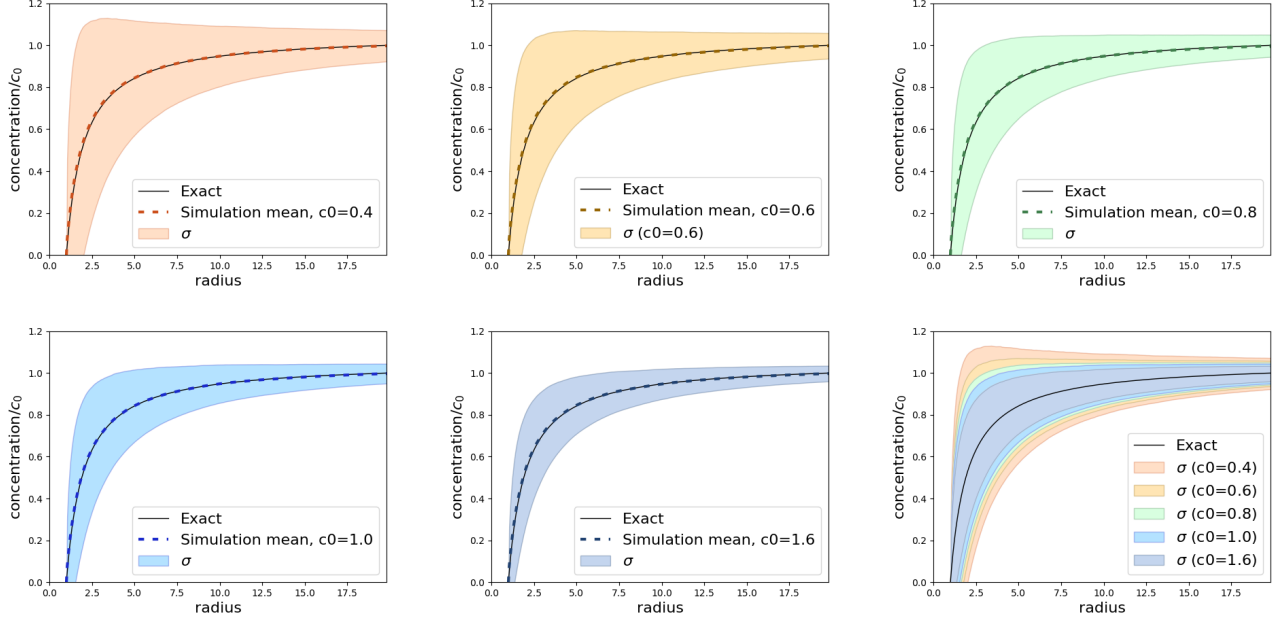


FIG. 3. Comparison between the exact solution of Smoluchowski's original concentration-based approach and particle-based simulations based on the GC-SME (purely-absorbing boundary). Results are plotted for five different values of the bath concentration $c_0 = [0.4, 0.6, 0.8, 1.0, 1.6]$; the standard deviation is represented by the shaded regions. The simulations were performed following the methodology described in Sec. IV, and they were averaged over 6×10^6 time steps, with $D = 5$, $dt = 0.0002$, $\sigma = 1$ and $r_{\max} = 20$. The results were normalized dividing by c_0 , so these graphs are representative of $\mathcal{N}_j^{\text{fr}}$ (see Appendix C). The last plot shows the standard deviations for the five concentrations on top of each other for comparison. This is a visual representation of the two different types of convergence: the mean field convergence from the hydrodynamic limit, where the mean matches the exact solution regardless of the bath state concentration; and the large copy number limit convergence (Eq. (C.3)), where the standard deviation is consistently reduced as the total number of particles increases ($c_0 \rightarrow \infty$).

following a Poisson process with a constant rate along with a first-order exit rate; this is physically consistent with the modeling of diffusion with a Markov model.

C. Emergent macroscopic chemical potential

The chemical potential summarizes the thermodynamics arising from diffusion and reaction in a chemical system. Deriving the chemical potential for diffusion-influenced reactions could help reconcile nonequilibrium thermodynamics with chemical reactions [46].

In order to derive the chemical potential, we begin by calculating a generalized version of Gibbs equilibrium free energy [47, 48]

$$\phi^{ss} = -k_B T \ln P^{ss},$$

where P^{ss} is the steady-state probability distribution, k_B is the Boltzmann constant and T the temperature. We will first calculate this function in terms of the number of particles, and then we will proceed to a concentration description. We substitute the (nonequilibrium) steady state distribution $P^{ss}(n_0, n_1, \dots, n_N)$, which in the Appendix C is shown to satisfy Eq. (C.1). As this is only a product of marginal dis-

tributions, we can expand it as

$$\phi^{ss}(n_0, n_1, \dots, n_N) = -k_B T \sum_{i=0}^N \ln(P^{ss}(n_i)), \quad (3.19)$$

where $P^{ss}(n_i) = \langle n_i \rangle e^{-\langle n_i \rangle} / n_i!$ is the marginal steady state probability of having n_i particles on shell i at time t . We can do a continuous interpolation by using the gamma function instead of the factorial (note the integral of the continuous distribution integrates to one),

$$P^{ss}(n_i) = \frac{\langle n_i \rangle^{n_i}}{\Gamma[n_i + 1]} e^{-\langle n_i \rangle} \approx \frac{1}{\sqrt{2\pi}} \left[\frac{\langle n_i \rangle}{n_i} \right]^{n_i} e^{n_i - \langle n_i \rangle}$$

where for the second equality we simply used Stirling's approximation $\Gamma(k+1) \approx \sqrt{2\pi k} (k/e)^k$ and $n_i + 1/2 \approx n_i$, which are both valid for $n_i \gg 1$. Inserting this again into Eq. (3.19), we obtain

$$\begin{aligned} \phi^{ss}(n_0, n_1, \dots, n_N) &\approx -k_B T \sum_{i=0}^N \ln \left(\frac{1}{\sqrt{2\pi}} \left[\frac{\langle n_i \rangle}{n_i} \right]^{n_i} e^{n_i - \langle n_i \rangle} \right) \\ &\approx k_B T \sum_{i=0}^N n_i \ln \left(\frac{n_i}{\langle n_i \rangle} \right) - n_i + \langle n_i \rangle + \ln \sqrt{2\pi}. \end{aligned}$$

As this is an energy, the last term is just an irrelevant constant factor. Furthermore, the number of particles n_i , can be simply

written in terms of the volume and concentration at shell i , $n_i = V_i c_i$, so we can rewrite the equation as a function of the volumes and concentrations,

$$\phi^{ss}(V_0, c_0, \dots, V_N, c_N) \approx k_B T \sum_{i=0}^N V_i \left[c_i \ln \left(\frac{c_i}{\langle c_i \rangle} \right) + \langle c_i \rangle - c_i \right].$$

As the chemical potential is nothing more than the derivative of the free energy with respect the concentration, $\mu(c_i) = \partial/\partial c_i(\phi(V_1, c_1, \dots, V_N, c_N))$, we simply obtain that the chemical potential at shell i is

$$\mu(c_i) \approx k_B T \ln \left(\frac{c_i}{\langle c_i \rangle} \right)^{V_i},$$

where $\langle c_i \rangle = \int_{r_i}^{r_i+\delta r} 4\pi r_i^2 c(r) dr$ and $c(r)$ is the solution to the original Smoluchowski equation for the concentration, Eq. (2.1). The quantity $(c_i/\langle c_i \rangle)^{V_i}$ plays the role of the thermodynamic activity in this model. Note the chemical potential dependence on V_i is necessary since the chemical potential depends on the spatial partition chosen and of the volume of each shell in the partition (the concept of defining thermodynamic quantities on partitions follows from nonequilibrium thermodynamics theory). If we include the boundaries, the far-field boundary satisfies $c_{N+1} = \langle c_{N+1} \rangle$ and consequently $\mu(c_{N+1})=0$. On the other hand, the reaction boundary only absorbs molecules, which leads to $\langle c_{-1} \rangle = \infty$ and $\mu(c_{-1}) = -\infty$. The systems is clearly a nonequilibrium open system driven by a chemical potential difference between the material bath and the absorbing boundary.

This result bridges the concept of chemical potential at a probabilistic level to a framework of densities, as previously done in [47, 48]. However, this work takes it a step further establishing this connection in a spatially inhomogeneous system with a simple reaction process.

One should note that the most relevant quantity is not the chemical potential *per se* but the chemical potential difference. To establish the difference appropriately, we need to use a consistent partition across the different states. For instance, consider partitions with either radial intervals of equal length or equal volume in every shell. In the latter case, the volume becomes irrelevant for the chemical potential difference. Both partitions would yield different chemical potential differences, but they would both describe correct dynamics in their corresponding coordinates.

IV. PARTICLE-BASED SIMULATIONS BASED ON THE GC-SME

In this section, we apply the previous results to produce arbitrary particle-based simulations coupled to a constant concentration material bath in the far-field. These simulations will be based on the GC-SME from III. Therefore, we consider a system where the mean far-field ($r > R$) concentration c_0 of B particles is constant. We incorporate one A particle at the origin with a purely absorbing reactive boundary at $r = \sigma$ surrounded by spherical shells of width δr and an additional outer shell in the region $r \in [R, R + \delta r]$ to model the material bath. Analogous to the chemical master equation, we can write the trajectory representation (Kurtz representation [33, 34, 49]) of the GC-SME, which tracks the dynamics of

the number of B particles $n_i(t)$ in shell i ,

$$n_i(t + \tau) = n_i(t) + \mathcal{R}_i(\{\bar{n}(t)\}, \tau),$$

where $\mathcal{R}(\{\bar{n}(t)\}, \tau)$ denotes the random change in the number of particles in shell i and $\{\bar{n}(t)\}$ is the set of elements $n_i(t)$ for every possible shell i . Naturally, it depends on the time interval τ and the current state of the system $\{\bar{n}(t)\}$. The process $\mathcal{R}_i(\{\bar{n}(t)\}, \tau)$ is a composition of two processes:

- The diffusion of B particles in the system, $\mathcal{D}_i(\{\bar{n}(t)\}, \tau)$, which includes diffusion across shells, reaction by diffusion into the absorbing boundary ($r = \sigma$) and diffusion out of the system into $r > R$.
- The injection of B particles coming from the material bath (outer shell) into the system, $\mathcal{I}_i(\{\bar{n}(t)\}, \tau)$.

These two processes are in general coupled and can occur at different time-scales, so the time integration requires a robust scheme, like Strang splitting [50]. The Strang splitting of $\mathcal{R}_i(\{\bar{n}(t)\}, \delta t)$ for one time step δt separates the diffusion step and the injection step as follows

$$\begin{aligned} n_i^* &= n_i(t) + \mathcal{I}_i(\{\bar{n}(t)\}, \delta t/2) \\ n_i^{**} &= n_i^* + \mathcal{D}_i(\{\bar{n}^*\}, \delta t) \\ n_i(t + \delta t) &= n_i^{**} + \mathcal{I}_i(\{\bar{n}^{**}\}, \delta t/2). \end{aligned} \quad (4.20)$$

A. Diffusion step

We would like that this method is extendable to arbitrary reaction-diffusion particle-based simulations without spherical symmetry. Therefore, we need to remove the constraint that the diffusion (and reaction) in $r < R$ is modeled through jumps between spherical shells. In order to do so, the diffusion step in the Strang splitting algorithm can be done through a particle-based simulation, like over-damped Langevin dynamics $dX_t = \sqrt{2D}dW_t$, with W_t a three-dimensional Wiener process, as commonly is the case in reaction-diffusion particle-based simulations [10, 51, 52], see [53] for an overview. This can be integrated with the Euler-Maruyama scheme [54] for each particle

$$X_j(t + \delta t) = X_j(t) + \sqrt{2D}\mathcal{N}(0, \delta t), \quad (4.21)$$

where D is the diffusion coefficient and $\mathcal{N}(0, \delta t)$ a three-dimensional vector with each entry a normal random variable with mean zero and variance δt , and j runs over all the B particles in the system. Note the number of B particles is not constant over time and that the diffusion coefficient satisfies the Einstein relation, $D = k_B T \beta$, where k_B is the Boltzmann constant, T the temperature and β a constant related to the damping. If a particle diffuses into an absorbing boundary (reaction) or into the region $r > R$, it is no longer considered part of the system. We chose to use an absorbing boundary (one absorbing A fixed at the origin) in order to verify the numerical scheme with the analytic solution. However, as the reaction-diffusion process is no longer restricted to spherical shells, the reaction-diffusion particle-based simulation in $r < R$ can be arbitrary; we could have chosen many diffusing reactive A 's as well.

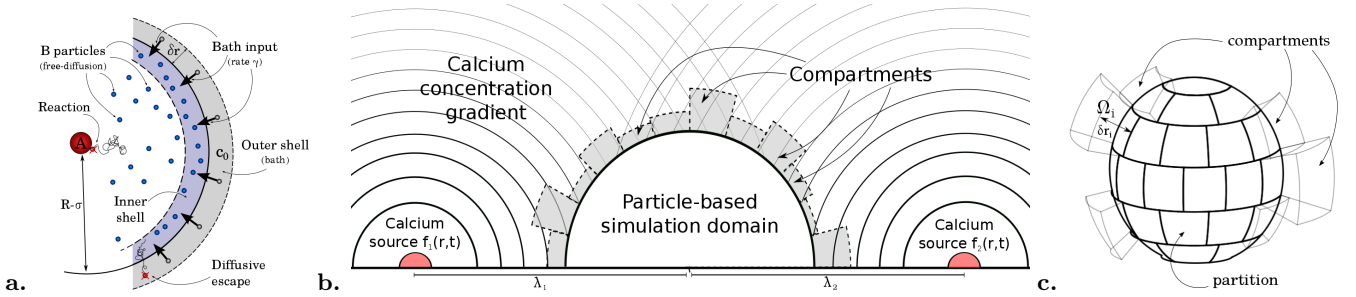


FIG. 4. Diagrams of particle-based simulations based on the GC-SME. **a.** Diagram of a two-dimensional slice of the particle-based simulation of Smoluchowski's model with constant concentration in the far-field from Sec. IV. The gray-shaded shell $(R, R + \delta r]$ represents the material bath, where n_{c_0} particles can jump into the system at every time step. The blue-shaded shell $(R - \delta r, R]$ delimits where the particles from the bath can jump into. The B particles (blue) can diffuse freely following standard Brownian motion in $[\sigma, R]$. If a B particle hits the reactive boundary at σ or escapes to $r > R$, it is eliminated. **b.** Diagram of a two-dimensional slice of the model implemented in Sec. V. Two sources placed at a distance λ_1 and λ_2 from the origin represent the calcium channels, which generate a concentration gradient in the intracellular space. The particle-based simulation is delimited by a half sphere surrounded by the compartments that define the material bath. Each compartment has a number of particles inside n_i that matches the corresponding average concentration in the compartment at a given time. The compartments volumes vary to keep n_i an integer. **c.** Three-dimensional illustration of the particle-based simulation boundary showing an equal area partition of the half-sphere. Each element of the partition has a corresponding δr_i , which generates compartments with volume Ω_i to define the material bath. For the sake of clarity, only a few compartments are shown, and the compartment size variation is exaggerated.

B. Injection step

In order to implement the injection of particles from the material bath, it is convenient to adhere to the shell description. However, it is only necessary to define two shells, the inner shell inside the system $r \in (R - \delta r, R]$ and the outer shell $r \in (R, R + \delta r]$, see Fig. 4a. The number of B particles in the outer shell n_{c_0} has to be consistent with the far-field concentration c_0 , i.e we need to find reasonable value of δr and n_{c_0} such that

$$c_0 = \frac{3n_{c_0}}{4\pi((R + \delta r)^3 - R^3)}. \quad (4.22)$$

As δr is constrained by the time step of the simulation by $2D\delta t \leq \delta r^2$ [11], we choose an initial guess for δr value slightly bigger than $\sqrt{2D\delta t}$. We further choose n_{c_0} as $4\pi c_0((R + \delta r)^3 - R^3)/3$ rounded up to the closest integer, and we do a Newton iteration on Eq. (4.22) as a function of δr . This will yield the volume (δr) in which an integer number of particles yield the concentration c_0 in the bath. It is important to check the time-step constraint is fulfilled; if it is not, we require a higher value for the initial guess of δr , which yields a larger n_{c_0} and consequently a larger δr . This method will determine the number of “virtual” particles in the outer shell (bath) and a consistent value for δr .

The “virtual” particles are injected from the bath (outer shell $(R, R + \delta r]$) into the inner shell $(R - \delta r, R]$. Each particle can jump inside with rate $\gamma(\delta r)$, as established in Eq. (3.18). Note we write $\gamma(\delta r)$ to emphasize that γ depends on the chosen δr . The locations of the particles injected into the system are somewhere within $(R - \delta r, R]$. As the exact location of the particles is unknown due to the discrete resolution of the GC-SME, it is reasonable to choose the location uniformly along $(R - \delta r, R]$. Once the particles are injected into the system, they can diffuse following the diffusion step.

C. The particle-based scheme based on the GC-SME

The scheme described in Sec. IV is depicted in Fig. 4a, and it is implemented as follows:

Input: Bath concentration c_0 , diffusion coefficient D , absorbing boundary σ , domain size R , time-step δt , initial guess for δr , total number of time iterations m and Newton iteration tolerance ϵ .

1. Use Eq. (4.22) to calculate n_{c_0} (to its nearest integer) and then approximate concentration c_0^{num} for the given δr .
2. While $|c_0^{\text{num}} - c_0| > \epsilon$:
 - (a) $\delta r \leftarrow$ Newton iteration on Eq. (4.22).
 - (b) Recalculate c_0^{num} .
3. If $2D\delta t > \delta r$:
 - (a) Exit, use larger initial guess for δr .
4. For $t = [0, \delta t, \dots, m\delta t]$:
 - (a) Inject particles from outer shell into inner shell for half a time step with rate $\gamma(\delta r)$. Sample location of new particles uniformly along $(R - \delta r, R]$.
 - (b) Diffuse all particles for δt following the scheme from Eq. (4.21). If particles crossed the absorbing boundary at $r = \sigma$ or the system domain at $r = R$, remove them.
 - (c) Inject particles from outer shell into inner shell for half a time step with rate $\gamma(\delta r)$. Sample location of new particles uniformly along $(R - \delta r, R]$.

Note steps 4a, 4b and 4c correspond to the Strang-splitting from Eq. (4.20). The results of simulations using this scheme are shown in Fig. 3, where we further verify the numerical scheme by showing the simulation results are consistent with the analytic solution. These simulations were performed using a purely absorbing reaction boundary. Nonetheless, it is straightforward to extend the simulation to partially absorbing reaction boundaries or more complicated reaction-diffusion schemes since any particle-based scheme can be implemented in the diffusion step.

V. COUPLING PARTICLE AND CONCENTRATION-BASED SIMULATIONS: AN APPLICATION TO EXOCYTOSIS

In this section, we generalize the scheme from Sec. IV by introducing a scheme to couple arbitrary particle-based simulations with time and space-dependent bulk concentration in the far-field. The far-field dynamics could be known beforehand or obtained from another model, like reaction-diffusion PDEs without high-order reactions. Interesting applications of this scheme arise in intracellular biological processes triggered by changes in calcium concentration through voltage-gated calcium channels. Examples of such processes are secretion of endocrine and exocrine cells and synaptic transmission, both of which occur through exocytosis [55–57].

Exocytosis consists of the active transport of molecules out of the cell. The molecules to be transported are carried in vesicles towards the cell membrane, where the vesicle fuses with the membrane expelling all of its contents out of the cell. It is well known that exocytosis is mainly triggered by changes in calcium concentration triggered by voltage-gated calcium channels [57]. Considering that vesicle diameters are around $50nm$ or larger [55], the domain of interest for a particle-based simulation should be at least four times that size ($200nm$), which spans a volume of $8 \times 10^6 nm^3$. Calcium concentrations are very nonisotropic; in order to trigger exocytosis, local calcium concentrations between $20\mu M$ and $1mM$ are required. This depends on the specific process, endocrine secretion is around $27\mu M$ and synaptic transmission above $100\mu M$ [55]. This means that the number of particles in the volume of interest could be between one hundred and several thousand, or even more if the volume of interest is bigger. This number of particles is big enough to roughly describe the calcium profile by a bulk concentration; however, it is small enough that specific processes involving calcium molecules would require a particle-based simulation. In other words, it is ideal for a coupling like the one we are proposing.

A. The model

As a proof of concept, we begin with a simple model inspired in exocytosis. We assume there is a set of N_S calcium sources in the cell membrane, each one of them located at x_k and producing a calcium concentration gradient $f_k(x, t)$ (with $k = 1, 2, \dots, N_S$) in the intracellular space, Fig. 4b. In the far-field, we are not interested in high-resolution dynamics, so a concentration description in terms of a diffusion PDE is enough; this could potentially be obtained from experiments. In our case, the concentration gradient will simply be given

by the sum of solutions to diffusion PDEs with an initial concentration source at x_k ,

$$f_k(x, t) = (4\pi Dt)^{-3/2} \exp\left[-\frac{|x - x_k|^2}{4Dt}\right].$$

We delimit the region of interest by half a sphere around the membrane, Fig. 4b, where specific calcium-triggered process, like exocytosis, could occur. In this region, we can incorporate arbitrary particle-based reaction-diffusion simulations to model processes like exocytosis in more detail; however, we restrict ourselves to simple diffusion for verification purposes. Simulations in this region could also include more detailed dynamics via MSM/RD [58], where Markov state models (MSMs) [59–62] extracted from detailed molecular dynamics simulations are coupled to particle-based reaction diffusion (RD) simulations. A more realistic simulation of the membrane could also be implemented with the novel particle-based membrane model from [63]. We should also note it is theoretically possible to do a particle-based simulation or even a molecular dynamics simulation on the whole region. In practice however this might be unfeasible, impractical and likely unnecessary.

The main idea is to extend the model from Sec. IV by incorporating angular and time resolution into the far-field concentration value. In this case, we will also need an outer shell covering the half sphere. However, we will need to divide it into angular compartments, so we can emulate the space-dependent material bath produced by the calcium concentration gradient. The scheme is constructed in a similar manner to that of Sec. IV, but it is applied to each of the compartments.

We begin by making an equal area partition of the surface of the half sphere of radius R into p regions denoted by $i = 1, \dots, p$ (Fig. 4c). We introduce two parameters for each region, δr_i and n_i . The first corresponds to the width that generates a compartment N_i of volume Ω_i , and the second corresponds to the number of particles inside that compartment. Note each of the compartments, N_1, \dots, N_p , has a different width δr_i , so it is delimited by $(R, R + \delta r_i]$, Fig. 4c. Given a reasonable initial guess of δr_i , we can estimate the volume of each compartment as $2\pi R^2 \delta r_i$ (an exact calculation is also possible), and we can obtain a relation for the bulk concentration c_i in each compartment at time t as

$$c_i(t) = \frac{1}{\Omega_i} \int_{\omega_i} \left(\sum_{k=1}^{N_S} f_k(x, t) \right) d\omega_i. \quad (5.23)$$

With the implementation of the compartments, the PDE solution for the far-field and this relation, we can derive the numerical scheme.

B. Generalized particle-based scheme

The scheme follows analogously from the Sec IV. It will also be divided in a diffusion and injection step; however, in order to model the time and space-dependent far-field concentration dynamics, this algorithm needs to consider each of the compartments, and requires the additional assumption that the bulk concentration changes slowly over one time step δt . Note that, although the diffusion step only implements particle diffusion, it can be extended to arbitrary particle-based reaction-diffusion simulations.

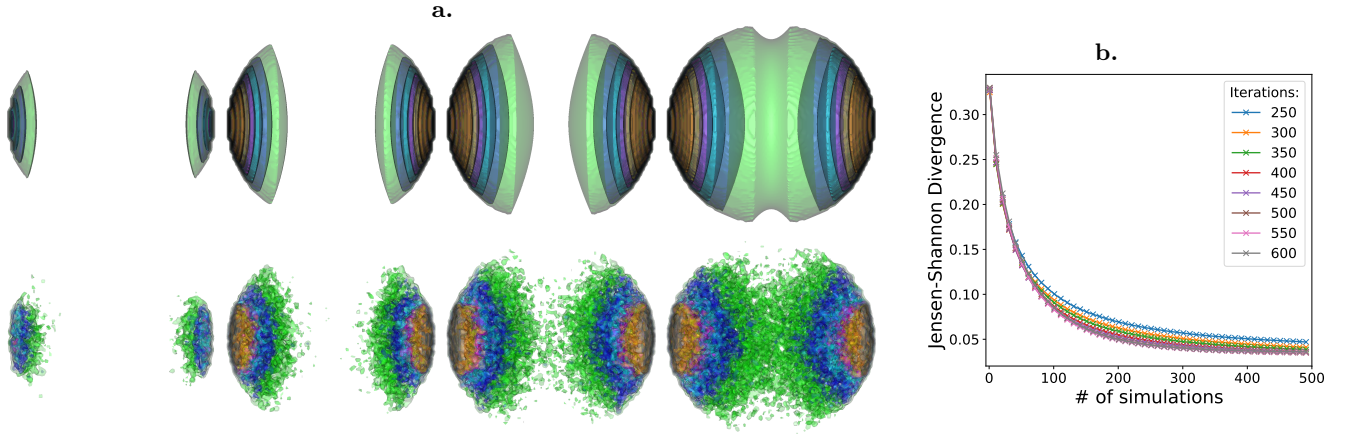


FIG. 5. **a.** Contour plots of the Calcium concentration profile observed from below the half sphere. The top plots correspond to the reference based on bulk concentration dynamics while the bottom ones correspond to the ensemble average of 200 particle-based simulations. Both simulations are plotted at four different points in time, 150, 250, 350 and 450 time iterations. Darker colors correspond to higher concentrations. **b.** Plot of the Jensen-Shannon divergence between the reference concentration histogram and the ensemble average concentration histogram (over particle simulations) as a function of the number of simulations used to calculate the ensemble average. This curve is plotted to compare the histograms at different times from 250 to 650 iterations. A value closer to zero means the histograms are closer to each other. As more simulations are used to calculate the average, we can observe the particle-based simulations are in quantitative statistical agreement with the bulk concentration dynamics.

Input: Bath concentration c_0 , diffusion coefficient D , absorbing boundary σ , domain size R , time-step δt , initial guesses for δr_i , total number of time iterations m , Newton iteration tolerance ϵ , partition chosen for compartments Ω_i and averaged bulk concentration function in compartments $c_i(t)$.

For $t = [0, \delta t, \dots, m\delta t]$:

1. For every compartment $i = 1, \dots, N_p$:
 - (a) Use Eq. (5.23) to calculate n_i (to its nearest integer) and then approximate concentration $c_i(t)^{\text{num}}$ for the given δr_i .
 - (b) While $|c_i^{\text{num}}(t) - c_i(t)| > \epsilon$:
 - $\delta r_i \leftarrow$ Newton iteration on Eq. (5.23).
 - Recalculate $c_i^{\text{num}}(t)$.
 - (c) If $2D\delta t > \delta r_i$:
 - Use a larger initial guess for δr_i and repeat 1.a and 1.b for current compartment.
2. For every compartment $i = 1, \dots, N_p$:
 - (a) Inject particles from compartment i into system for half a time step with rate $\gamma_i(\delta r_i)$. Sample location of new particles uniformly in the region delimited by the partition i and $(R - \delta r_i, R]$.
3. Diffuse all particles for δt following the scheme from Eq. (4.21). If particles crossed the system domain at $r = R$, remove them.
4. For every compartment $i = 1, \dots, N_p$:

- (a) Inject particles from compartment i into system for half a time step with rate $\gamma_i(\delta r_i)$. Sample location of new particles uniformly in the region delimited by the partition i and $(R - \delta r_i, R]$.

Following the setup from Fig. 4b, we illustrate the results for a "proof of concept" simulation with two sources for the Calcium concentration at distances $\lambda_1 = \lambda_2 = 5$ from the origin. Fig. 5a shows the concentration contour plots in the half-sphere region (with radius $R = 5$) (seen from below) for an average of 200 particle-based simulation along with the reference bulk concentration solution at four different times. Furthermore, we compared the three-dimensional concentration histograms obtained from the particle-based simulations ensemble averages against the reference concentration solutions. The similarity between the two distributions was measured by calculating the Jensen-Shannon divergence [64] between the two normalized concentration histograms; Fig. 5b shows this comparison as a function of the number of simulations used to calculate the ensemble average at different points in time. We observe the particle-based simulation are in quantitative statistical agreement with the bulk concentration dynamics, which validates the simulation results. Although we constructed this scheme with exocytosis applications in mind, it could be implemented for many other systems.

Note it is straightforward to extend the bulk concentration description to include several species and unimolecular reactions, where the dynamics are in terms of reaction-diffusion PDEs restricted to first-order reactions. Extending the scheme to incorporate higher-order reactions in the coupling boundary is not trivial since higher-order reactions are no longer independent of diffusion. This is also an issue in [25]; however, we think the GC-SME provides a robust framework that will be helpful to address this issue in future work. Nonetheless, the current scheme can be generalized to arbitrarily complicated systems in the particle-based region.

VI. CONCLUSION

We constructed continuous-time discrete-state Markov models for diffusion-influenced reactions (SMEs). The first SME corresponds to the case of an isolated pair of reacting particles. In the continuous limit, it recovers Smoluchowski’s probabilistic approach. We later introduced the GC-SME, a generalization of the previous SME to an arbitrary non-constant number of ligand particles. In the continuous limit, when taking either the hydrodynamic or the large copy number limit, the GC-SME converges to Smoluchowski’s concentration-based approach with a constant concentration in the far-field. We finally employed this result to implement two particle-based simulations coupled to bulk concentration descriptions.

The GC-SME convergence result addresses several matters of relevance to the theory of diffusion-limited reactions and stochastic reaction-diffusion processes. First of all, it establishes a precise connection between the probabilistic and concentration-based approach as well as an interpretation of the concentration-based approach in terms of a probabilistic model; this is essentially an extension of Kurtz limit [33, 34] to a class of spatially inhomogeneous chemical systems. In addition, it provides a robust framework for statistical mechanical interpretation, which clarifies interpretations at the

particle level and bridges the concept of chemical potential from a mesoscopic to a macroscopic scale. In a more pragmatic note, it enables multiscale and hybrid particle-based schemes by consistently coupling them to reaction-diffusion PDEs (with only first-order reactions).

The results in this paper provide the blueprints for multiscale/hybrid numerical frameworks that could potentially couple particle-based reaction-diffusion simulations with general reaction-diffusion PDEs. However, our current approach only allows for higher-order reactions to occur inside the particle-based domain since it can only couple diffusion processes across the particle-based simulation boundary. Therefore, it is not yet clear how can one couple high-order reaction processes consistently. We leave this endeavor for future work.

VII. ACKNOWLEDGMENTS

We gratefully acknowledge support by the Deutsche Forschungsgemeinschaft (grants SFB1114, projects C03 and A04), the Einstein Foundation Berlin (ECMath grant CH17), the European research council (ERC starting grant 307494 “pcCell”) and the National Science and Technology Council of Mexico (CONACYT). We also thank Attila Szabo for insightful discussions and encouragements over the course of this work.

-
- [1] F. C. Collins and G. E. Kimball, “Diffusion-controlled reaction rates,” *J. Colloid Sci.*, vol. 4, no. 4, pp. 425–437, 1949.
 - [2] M. von Smoluchowski, “Versuch einer mathematischen theorie der koagulationskinetik kolloider lösungen,” *Z. Phys. Chem.*, vol. 92, no. 129-168, p. 9, 1917.
 - [3] N. Agmon and A. Szabo, “Theory of reversible diffusion-influenced reactions,” *J. Chem. Phys.*, vol. 92, no. 9, pp. 5270–5284, 1990.
 - [4] P. Hänggi, P. Talkner, and M. Borkovec, “Reaction-rate theory: Fifty years after Kramers,” *Rev. Mod. Phys.*, vol. 62, no. 2, p. 251, 1990.
 - [5] J. Keizer, “Nonequilibrium statistical thermodynamics and the effect of diffusion on chemical reaction rates,” *The Journal of Physical Chemistry*, vol. 86, no. 26, pp. 5052–5067, 1982.
 - [6] —, “Diffusion effects on rapid bimolecular chemical reactions,” *Chemical Reviews*, vol. 87, no. 1, pp. 167–180, 1987.
 - [7] J. M. Schurr, “The role of diffusion in bimolecular solution kinetics,” *Biophys. J.*, vol. 10, no. 8, p. 700, 1970.
 - [8] A. Szabo, K. Schulten, and Z. Schulten, “First passage time approach to diffusion controlled reactions,” *J. Chem. Phys.*, vol. 72, no. 8, pp. 4350–4357, 1980.
 - [9] A. Szabo, “Theory of diffusion-influenced fluorescence quenching,” *J. Phys. Chem.*, vol. 93, no. 19, pp. 6929–6939, 1989.
 - [10] M. J. Del Razo, W. Pan, H. Qian, and G. Lin, “Fluorescence correlation spectroscopy and nonlinear stochastic reaction–diffusion,” *The Journal of Physical Chemistry B*, vol. 118, no. 25, pp. 7037–7046, 2014.
 - [11] M. J. del Razo and H. Qian, “A discrete stochastic formulation for reversible bimolecular reactions via diffusion encounter,” *Comm. Math. Sci.*, vol. 14, no. 6, pp. 1741–1772, 2016.
 - [12] N. Dorsaz, C. De Michele, F. Piazza, P. De Los Rios, and G. Foffi, “Diffusion-limited reactions in crowded environments,” *Phys. Rev. Lett.*, vol. 105, no. 12, p. 120601, 2010.
 - [13] A. Donev, V. V. Bulatov, T. Oettel, G. H. Gilmer, B. Sadigh, and M. H. Kalos, “A first-passage kinetic monte carlo algorithm for complex diffusion–reaction systems,” *J. Comput. Phys.*, vol. 229, no. 9, pp. 3214–3236, 2010.
 - [14] I. V. Gopich and A. v. Szabo, “Kinetics of reversible diffusion influenced reactions: the self-consistent relaxation time approximation,” *J. Chem. Phys.*, vol. 117, no. 2, pp. 507–517, 2002.
 - [15] S. J. Hagen, J. Hofrichter, A. Szabo, and W. A. Eaton, “Diffusion-limited contact formation in unfolded cytochrome c: estimating the maximum rate of protein folding,” *Proc. Natl. Acad. Sci. U.S.A.*, vol. 93, no. 21, pp. 11 615–11 617, 1996.
 - [16] B. Peters, P. G. Bolhuis, R. G. Mullen, and J.-E. Shea, “Reaction coordinates, one-dimensional Smoluchowski equations, and a test for dynamical self-consistency,” *J. Chem. Phys.*, vol. 138, no. 5, p. 054106, 2013.
 - [17] T. Prüstel and M. Meier-Schellersheim, “Theory of reversible diffusion-influenced reactions with non-Markovian dissociation in two space dimensions,” *J. Chem. Phys.*, vol. 138, no. 10, p. 104112, 2013.
 - [18] K. Tucci and R. Kapral, “Mesoscopic model for diffusion-influenced reaction dynamics,” *J. Chem. Phys.*, vol. 120, no. 17, pp. 8262–8270, 2004.
 - [19] A. Vijaykumar, P. G. Bolhuis, and P. R. ten Wolde, “Combining molecular dynamics with meso-

- sopic Green's function reaction dynamics simulations," *J. Chem. Phys.*, vol. 143, no. 21, p. 214102, 2015.
- [20] A. Vijaykumar, T. E. Ouldridge, P. R. ten Wolde, and P. G. Bolhuis, "Multiscale simulations of anisotropic particles combining molecular dynamics and Green's function reaction dynamics," *J. Chem. Phys.*, vol. 146, no. 11, p. 114106, 2017.
- [21] J. S. van Zon and P. R. Ten Wolde, "Green's-function reaction dynamics: A particle-based approach for simulating biochemical networks in time and space," *J. Chem. Phys.*, vol. 123, no. 23, p. 4910, 2005.
- [22] A. Szabo, "Autobiography of Attila Szabo," *J. Phys. Chem. B*, vol. 112, no. 19, pp. 5883–5891, 2008.
- [23] O. G. Berg, "On diffusion-controlled dissociation," *Chem. Phys.*, vol. 31, no. 1, pp. 47–57, 1978.
- [24] I. V. Gopich and A. Szabo, "Asymptotic relaxation of reversible bimolecular chemical reactions," *Chem. Phys.*, vol. 284, no. 1-2, pp. 91–102, 2002.
- [25] B. Franz, M. B. Flegg, S. J. Chapman, and R. Erban, "Multiscale reaction-diffusion algorithms: PDE-assisted Brownian dynamics," *SIAM J. Appl. Math.*, vol. 73, no. 3, pp. 1224–1247, 2013.
- [26] S. Smith and R. Grima, "Spatial stochastic intracellular kinetics: A review of modelling approaches," *Bull. Math. Biol.*, pp. 1–50, 2018.
- [27] M. Doi, "Stochastic theory of diffusion-controlled reaction," *J. Phys. A: Math. Gen.*, vol. 9, no. 9, p. 1479, 1976.
- [28] R. Erban and S. J. Chapman, "Stochastic modelling of reaction–diffusion processes: algorithms for bimolecular reactions," *Phys. Biol.*, vol. 6, no. 4, p. 046001, 2009.
- [29] S. A. Isaacson, "The reaction-diffusion master equation as an asymptotic approximation of diffusion to a small target," *SIAM J. Appl. Math.*, vol. 70, no. 1, pp. 77–111, 2009.
- [30] —, "A convergent reaction-diffusion master equation," *J. Chem. Phys.*, vol. 139, no. 5, p. 054101, 2013.
- [31] T. Franco, "Interacting particle systems: hydrodynamic limit versus high density limit," in *From Particle Systems to Partial Differential Equations*. Springer, 2014, pp. 179–189.
- [32] C. Kipnis and C. Landim, *Scaling limits of interacting particle systems*. Springer Science & Business Media, 2013, vol. 320.
- [33] T. G. Kurtz, "Limit theorems for sequences of jump Markov processes approximating ordinary differential processes," *J. Appl. Probab.*, vol. 8, no. 2, pp. 344–356, 1971.
- [34] T. G. v. Kurtz, "The relationship between stochastic and deterministic models for chemical reactions," *J. Chem. Phys.*, vol. 57, no. 7, pp. 2976–2978, 1972.
- [35] H. Qian and L. M. Bishop, "The chemical master equation approach to nonequilibrium steady-state of open biochemical systems: linear single-molecule enzyme kinetics and nonlinear biochemical reaction networks," *Int. J. Mol. Sci.*, vol. 11, no. 9, pp. 3472–3500, 2010.
- [36] B. Corry, S. Kuyucak, and S.-H. Chung, "Tests of continuum theories as models of ion channels. ii. poisson–planck theory versus Brownian dynamics," *Biophys. J.*, vol. 78, no. 5, pp. 2364–2381, 2000.
- [37] M. G. Pedersen, G. Cortese, and L. Eliasson, "Mathematical modeling and statistical analysis of calcium-regulated insulin granule exocytosis in β -cells from mice and humans," *Prog. Biophys. Mol. Biol.*, vol. 107, no. 2, pp. 257–264, 2011.
- [38] P. I. Zhuravlev and G. A. Papoian, "Molecular noise of capping protein binding induces macroscopic instability in filopodial dynamics," *Proc. Natl. Acad. Sci. U.S.A.*, vol. 106, no. 28, pp. 11 570–11 575, 2009.
- [39] W. J. Heuett and H. Qian, "Grand canonical Markov model: a stochastic theory for open nonequilibrium biochemical networks," *J. Chem. Phys.*, vol. 124, no. 4, p. 044110, 2006.
- [40] D. Shoup and A. Szabo, "Role of diffusion in ligand binding to macromolecules and cell-bound receptors," *Biophys. J.*, vol. 40, no. 1, pp. 33–39, 1982.
- [41] T. Sokolowski, L. Bossen, T. Miedema, and N. Becker, "Green's function reaction dynamics—an exact and efficient way to simulate intracellular pattern formation," in *ICNAAM 2010*, vol. 1281, no. 1. AIP Publishing, 2010, pp. 1342–1345.
- [42] J. S. van Zon and P. R. Ten Wolde, "Simulating biochemical networks at the particle level and in time and space: Green's function reaction dynamics," *Phys. Rev. Lett.*, vol. 94, no. 12, p. 128103, 2005.
- [43] F. X.-F. Ye, P. Stinis, and H. Qian, "Dynamic looping of a free-draining polymer," *SIAM J. Appl. Math.*, vol. 78, no. 1, pp. 104–123, 2018.
- [44] H. Wang, C. S. Peskin, and T. C. Elston, "A robust numerical algorithm for studying biomolecular transport processes," *J. Theor. Biol.*, vol. 221, no. 4, pp. 491–511, 2003.
- [45] R. Pathria and P. Beale, *Statistical Mechanics*. Elsevier Science, 1996.
- [46] D. Bedeaux, I. Pagonabarraga, J. O. De Zárata, J. Sengers, and S. Kjelstrup, "Mesoscopic non-equilibrium thermodynamics of non-isothermal reaction-diffusion," *Phys. Chem. Chem. Phys.*, vol. 12, no. 39, pp. 12 780–12 793, 2010.
- [47] H. Ge and H. Qian, "Mesoscopic kinetic basis of macroscopic chemical thermodynamics: A mathematical theory," *Phys. Rev. E*, vol. 94, no. 5, p. 052150, 2016.
- [48] H. Ge and H. v. Qian, "Mathematical formalism of nonequilibrium thermodynamics for nonlinear chemical reaction systems with general rate law," *J. Stat. Phys.*, vol. 166, no. 1, pp. 190–209, 2017.
- [49] D. F. Anderson and T. G. Kurtz, *Stochastic analysis of biochemical systems*. Springer, 2015, vol. 1.
- [50] C. Kim, A. Nonaka, J. B. Bell, A. L. Garcia, and A. Donev, "Stochastic simulation of reaction-diffusion systems: A fluctuating-hydrodynamics approach," *J. Chem. Phys.*, vol. 146, no. 12, p. 124110, 2017.
- [51] S. S. Andrews and D. Bray, "Stochastic simulation of chemical reactions with spatial resolution and single molecule detail," *Phys. Biol.*, vol. 1, no. 3, p. 137, 2004.
- [52] J. Schöneberg and F. Noé, "Readdy—a software for particle-based reaction-diffusion dynamics in crowded cellular environments," *PLoS one*, vol. 8, no. 9, p. e74261, 2013.
- [53] J. Schöneberg, A. Ullrich, and F. Noé, "Simulation tools for particle-based reaction-diffusion dynamics in continuous space," *BMC biophysics*, vol. 7, no. 1, p. 11, 2014.
- [54] D. J. Higham, "An algorithmic introduction to numerical simulation of stochastic differential equations," *SIAM review*, vol. 43, no. 3, pp. 525–546, 2001.
- [55] S. M. Bajjalieh and R. H. Scheller, "The biochemistry of neurotransmitter secretion," *J. Biol. Chem.*, vol. 270, no. 5, pp. 1971–1974, 1995.

- [56] S. Barnes and M. E. Kelly, “Calcium channels at the photoreceptor synapse,” in *Photoreceptors and calcium*. Springer, 2002, pp. 465–476.
- [57] W. A. Catterall, “Voltage-gated calcium channels,” *Cold Spring Harb. Perspect. Biol.*, vol. 3, no. 8, p. a003947, 2011.
- [58] M. Dibak, M. J. del Razo, D. De Sancho, C. Schütte, and F. Noé, “MSM/RD: Coupling Markov state models of molecular kinetics with reaction-diffusion simulations,” *J. Chem. Phys.*, vol. 148, no. 21, p. 214107, 2018.
- [59] G. R. Bowman, V. S. Pande, and F. Noé, “Introduction and overview of this book,” in *An introduction to Markov state models and their application to long timescale molecular simulation*. Springer, 2014, pp. 1–6.
- [60] J.-H. Prinz, H. Wu, M. Sarich, B. Keller, M. Senne, M. Held, J. D. Chodera, C. Schütte, and F. Noé, “Markov models of molecular kinetics: Generation and validation,” *J. chem. phys.*, vol. 134, no. 17, p. 174105, 2011.
- [61] C. Schütte and M. Sarich, *Metastability and Markov state models in molecular dynamics: modeling, analysis, algorithmic approaches*. American Mathematical Soc., 2013, vol. 24.
- [62] B. Trendelkamp-Schroer, H. Wu, F. Paul, and F. Noé, “Estimation and uncertainty of reversible Markov models,” *J. chem. phys.*, vol. 143, no. 17, p. 11B601.1, 2015.
- [63] M. Sadeghi, T. R. Weigl, and F. Noé, “Particle-based membrane model for mesoscopic simulation of cellular dynamics,” *J. Chem. Phys.*, vol. 148, no. 4, p. 044901, 2018.
- [64] J. Lin, “Divergence measures based on the Shannon entropy,” *IEEE Trans. Inf. Theory*, vol. 37, no. 1, pp. 145–151, 1991.

Appendix A: Smoluchowski’s model with periodic flux

In addition to the models of Sec. II, we can also obtain a concentration-based Smoluchowski model in the canonical ensemble, i.e. where the total concentration of B is conserved. This is achieved by using a partially absorbing boundary condition and forcing a periodic flux. The corresponding boundary conditions for the Fokker-Planck equation (Eq. (2.1)) are,

$$4\pi\sigma^2 D \left. \frac{\partial f(r,t)}{\partial r} \right|_{r=\sigma} = 4\pi R^2 D \left. \frac{\partial f(r,t)}{\partial r} \right|_{r=R} = \kappa f(\sigma, t), \quad (\text{A.1})$$

and $\int_{\sigma}^R 4\pi r^2 f(r,t) dr = 1$. These conditions mean that the probability flux at $r = \sigma$ is the same as the flux at $r = R$. The steady state solution is exactly of the same form as Eq. (2.3), but with the constant A_0 instead of c_0 ,

$$f^{ss}(r) = A_0 \left[1 - \frac{\kappa\sigma}{4\pi D\sigma + \kappa} \left(\frac{1}{r} \right) \right], \quad (\text{A.2})$$

$$A_0 = \left[4\pi \left(\frac{R^3 - \sigma^3}{3} \right) - \frac{4\pi\sigma\kappa}{4\pi\sigma D + \kappa} \left(\frac{R^2 - \sigma^2}{2} \right) \right]^{-1}.$$

This result is a first step to provide a mathematical connection between the concentration-based approach and the probability approach. It can be easily interpreted as a concentration gradient for a large number of B molecules, where the absorption flux at σ is exactly the same as the incoming flux

of particle at $r = R$, but it can also be understood as the probability distribution for one B molecule, which every time it is absorbed at $r = \sigma$, it is placed back again at $r = R$.

We should note that the boundary condition in Eq. (A.1) is also satisfied in the original Collins and Kimball formulation at steady state from Eq. (2.3). However, in a probabilistic interpretation, the free parameter A_0 would give the normalization constant for the probability, which we can fix so the probability integrates to one.

Appendix B: Canonical Smoluchowski master equation

The SME derived in Sec. II C gives us the dynamics of the probability of one B molecule in this system. The quantity $\pi_i(t)$ is the probability of finding one B molecule in shell i at time t . In this section, we will obtain the SME in the canonical ensemble for an arbitrarily but fixed number of B molecules. We assume m independent and identical B molecules that obey Eq. (2.9). The number of ways to arrange m independent B molecules in the system, such that n_i are in state i (shell i) while maintaining the total number constant $m = n_1 + n_2 + \dots + n_N$, is given by the multinomial distribution [39]. Therefore, we can write the joint probability of having n_i molecules on each state simply as the multinomial

$$P(n_0, n_1, \dots, n_N, t) = \frac{m!}{n_0! n_1! \dots n_N!} \pi_0(t)^{n_0} \pi_1(t)^{n_1} \dots \pi_N(t)^{n_N}. \quad (\text{B.1})$$

Therefore, the expected value of having n_k molecules in shell k at time t is given by the expected value of the multinomial,

$$\mathbb{E}[\mathcal{N}_k = n_k] = m\pi_k(t), \quad (\text{B.2})$$

where \mathcal{N}_k refers to the random number of particles in shell k . We now show that the equation satisfied by this expected value in the continuous limit is the Smoluchowski’s equation (Eq. (2.1)) with the periodic boundary conditions from Eq. (A.1).

In the interest of minimizing notation, we will refer to the expected value of Eq. (B.2), $\mathbb{E}[\mathcal{N}_k = n_k]$, as $F_i(t) = m\pi_k(t)$. We want to establish a connection between this model and the original SME from Eq. (2.9). In order to do so, we only need to multiply by m the equation for the i^{th} shell given by Eq. (2.12). This yields

$$\frac{dF_i(t)}{dt} = q_{i+1,i} F_{i+1}(t) - (q_{i,i-1} + q_{1,i+1}) F_i(t) + q_{i-1,i} F_{i-1}(t). \quad (\text{B.3})$$

We will now follow a similar procedure to that of [11]. Substituting the corresponding values for the transition rates given in Eq. (2.11), we obtain the following equation

$$\frac{dF_i(t)}{dt} = D \left[\frac{F_{i+1}(t) - 2F_i(t) + F_{i-1}(t)}{\delta r^2} \right] - \frac{2D}{r_i} \left[\frac{F_{i+1}(t) - F_{i-1}(t)}{2\delta r} \right] + \frac{D}{\delta r} \left[\frac{F_i(t)}{r_i - \delta r} - \frac{F_i(t)}{r_i + \delta r} \right]. \quad (\text{B.4})$$

We can now take the limit as $\delta r \rightarrow 0$ to obtain

$$\begin{aligned} \frac{\partial F(r,t)}{\partial t} &= D \frac{\partial^2 F(r,t)}{\partial r^2} - \frac{2D}{r} \frac{\partial F(r,t)}{\partial r} + \frac{2D}{r^2} F(r,t), \\ &= D \frac{\partial^2 F(r,t)}{\partial r^2} - \frac{\partial}{\partial r} \left(\frac{2D}{r} F(r,t) \right), \end{aligned} \quad (\text{B.5})$$

where $F(r, t)dr$ is the continuous analog of $F_i(t)$, i.e. the expected value for the number of B particles in a shell of width δr in position r and at time t .

This is the expected value computed at any point in the shell with radius r , so we cannot yet compare it with the Smoluchowski diffusion equation. In order to do so, we need the equation for the expected value at any point in space given by $f(r, \theta, \phi, t)r^2 \sin(\theta)drd\theta d\phi$. Integrating this equation in the angular coordinates due to symmetry yields the expected value we just obtained, $F(r, t)$,

$$F(r, t)dr = 4\pi r^2 f(r, t)dr. \quad (\text{B.6})$$

Substituting this result into Eq. (B.5) and doing some algebra, we recover the Smoluchowski original equation, Eq. (2.1),

$$\frac{\partial f(r, t)}{\partial t} = \frac{D}{r^2} \frac{\partial}{\partial r} \left(r^2 \frac{\partial f(r, t)}{\partial r} \right).$$

Note that, in this case, the equation has a very precise meaning. The quantity $4\pi r^2 f(r, t)\delta r$ is the expected number of particles at the shell of radius r and width δr at time t . More precisely, the quantity $f(r, t)$ has units of number of particles per unit volume, so it is the expected value for the concentration at a given point with position r at time t .

We still need to deal with the boundary conditions. We can also obtain the equations at the boundaries by again multiplying by m the first and last equation of the system of Eqs. (2.9). The resulting equations for the inner and outer boundaries are the following,

$$\frac{dF_0(t)}{dt} = -(q_{0,1} + q_{0,b})F_0(t) + q_{1,0}F_1(t) \quad (\text{B.7})$$

$$\frac{dF_N(t)}{dt} = F_0(t)q_{0,b} + F_{N-1}(t)q_{N-1,N} - F_N(t)q_{N,N-1}$$

Note $q_{0,b} = \tilde{\kappa}(r)$, where the physically reasonable assumption is that the rate $\tilde{\kappa}(r)$ scales inversely to the infinitesimal volume of the reaction spherical shell, i.e. $\tilde{\kappa}(r) = \kappa/(4\pi r^2 \delta r)$, where κ will be the constant rate in the boundary condition [11].

Substituting the rates into the last two equations at the inner and outer boundary at shells $i = 0$ and $i = n$ and doing some algebra, we obtain the following equations for the inner boundary ,

$$\begin{aligned} \frac{dF_0}{dt} &= \frac{D}{\delta r^2} \left[F_1 - 2F_0 + F_0 \left(1 - \frac{\delta r^2}{D} \frac{\kappa}{4\pi r_0^2 \delta r} \right) \right] \\ &\quad - \left[\frac{D}{r_0} \frac{F_1}{\delta r} + \frac{D}{\delta r} \left(\frac{F_0}{r_0 + \delta r} \right) \right] \\ &= D \left[\frac{F_1 - 2F_0 + F_{-1}}{\delta r^2} \right] - \frac{2D}{r_0} \left[\frac{F_1 - F_{-1}}{2\delta r} \right] \\ &\quad + \frac{D}{\delta r} \left[\frac{F_0}{r_0 - \delta r} - \frac{F_0}{r_0 + \delta r} \right], \end{aligned} \quad (\text{B.8})$$

and for the outer boundary

$$\begin{aligned} \frac{dF_N}{dt} &= \frac{D}{\delta r^2} [F_{N-1} - 2F_N + F_N] \\ &\quad + \left[\frac{D}{r_N} \frac{F_{N-1}}{\delta r} + \frac{D}{\delta r} \left(\frac{F_N}{r_N - \delta r} \right) \right] - F_0 \frac{\kappa}{4\pi r_0^2 \delta r}, \\ &= D \left[\frac{F_{N-1} - 2F_N + F_{N+1}}{\delta r^2} \right] - \frac{2D}{r_N} \left[\frac{F_{N+1} - F_{N-1}}{2\delta r} \right] \\ &\quad + \frac{D}{\delta r} \left[\frac{F_N}{r_N - \delta r} - \frac{F_0}{r_N + \delta r} \right]. \end{aligned} \quad (\text{B.9})$$

Note we omitted the time dependence of $F_i(t)$ to simplify notation. In both cases, Eq. (B.8) and Eq. (B.9), we introduced the ghost cells F_{-1} and F_{N+1} respectively to force the equation to satisfy Eq. (B.4) (the equation satisfied inside the boundaries). In order for Eqs. (B.8) and (B.9) to be satisfied, the ghost cells need to satisfy the equations

$$\begin{aligned} F_0 - F_0 \frac{\kappa \delta r}{4\pi D r_0^2} &= F_{-1} + \frac{\delta r}{r_0} F_{-1} + \frac{\delta r}{r_0 - \delta r} F_0, \\ F_N - F_0 \frac{\kappa \delta r}{4\pi D r_0^2} &= F_{N+1} - \frac{\delta r}{r_N} F_{N+1} - \frac{\delta r}{r_N + \delta r} F_N, \end{aligned}$$

which will yield the boundary conditions. Arranging terms, dividing by δr and taking the limit as $\delta r \rightarrow 0$, we obtain

$$\begin{aligned} \left. \frac{\partial F(r, t)}{\partial r} \right|_{r=\sigma} &= \frac{\kappa}{4\pi D \sigma^2} F(\sigma, t) + \frac{F(\sigma, t)}{\sigma}, \\ \left. \frac{\partial F(r, t)}{\partial r} \right|_{r=r_{\max}} &= \frac{\kappa}{4\pi D \sigma^2} F(\sigma, t) + \frac{F(r_{\max}, t)}{r_{\max}}, \end{aligned}$$

respectively, where $r_0 = \sigma$ is the innermost shell and r_{\max} is the outermost shell. Applying once again the identity in Eq. (B.6), we obtain the boundary conditions for the Smoluchowski model with periodic flux from Appendix A,

$$\begin{aligned} 4\pi D \sigma^2 \left. \frac{\partial f(r, t)}{\partial r} \right|_{r=\sigma} &= \kappa f(\sigma, t), \\ 4\pi D r_{\max}^2 \left. \frac{\partial f(r, t)}{\partial r} \right|_{r=r_{\max}} &= \kappa f(\sigma, t). \end{aligned}$$

These are the boundary conditions for the expected value of the concentration at position r and time t . It should be noted that the process to obtain the continuous limit of these equations is analogous to the one we presented in [11].

This result shows that the Smoluchowski model with periodic flux from Appendix A is the mean field of Eq. (B.1), i.e. a number m of B molecules, each obeying Eq. (2.9). The model described by Eq. (B.1) provides a probabilistic approach to model concentration-based diffusion-influenced reactions. It not only yields the expected mean field but can also yield the full probability distribution for all particles.

The steady state of the probabilistic model from Eq. (B.1) is a nonequilibrium steady state since it always has a constant flux from the outer boundary into the inner one, so the total number of particles in the system does not change or fluctuate over time. Therefore, following statistical mechanics terminology, we say this system is in the canonical ensemble. Note the original Smoluchowski concentration-based model (Eq. (2.1)) does not maintain a constant number of particles (or concentration), unless the system is in steady state. Therefore, the model from Eq. (B.1) has limited applicability. Nonetheless, this is the first step to connect the probabilistic and concentration interpretations. For a general case, see Sec. III.

Appendix C: Large copy number limit

In this section, we show the large copy number limit of the GC-SME also recovers the concentration-based approach

from Sec. II A. We begin by pointing out that Eq. (3.14) is a particular case of the equation,

$$\frac{d\langle n_i(t) \rangle}{dt} = \sum_{\substack{j=-1 \\ j \neq i}}^{N+1} [\langle n_j(t) \rangle q_{j,i} - \langle n_i(t) \rangle q_{i,j}].$$

which corresponds to a generalized version of the master equation, Eq. (3.13), where all the states can interact with one another. In [39], it was shown that a solution to this general master equation satisfies the following Poisson probability distribution,

$$P(n_0, n_1, \dots, n_N, t) = \prod_{i=0}^N \left[\frac{\langle n_i(t) \rangle^{n_i}}{n_i!} e^{-\langle n_i(t) \rangle} \right]. \quad (\text{C.1})$$

This can be proved by direct substitution. As our equation is of the same form, it also satisfies the same distribution. Also note the expected value for the number of particles at shell i of this distribution is $\langle n_i(t) \rangle$. Taking the marginal distribution by integrating all except one of the variables, we obtain

$$P(\mathcal{N}_j = n_j, t) = \frac{\langle n_j(t) \rangle^{n_j}}{n_j!} e^{-\langle n_j(t) \rangle}. \quad (\text{C.2})$$

The random variable \mathcal{N}_j which gives the number of particles at each state/shell obeys a simple Poisson distribution. Now consider the scaling $\mathcal{N}_j^{\text{fr}} = \mathcal{N}_j/c_0$ (c_0 constant). The mean

and standard deviation for $\mathcal{N}_j^{\text{fr}}$ are then given by

$$\mu_j^{\text{fr}} = \frac{\langle n_j(t) \rangle}{c_0} \quad \sigma_j^{\text{fr}} = \frac{\langle n_j(t) \rangle}{c_0}$$

Using Chebyshev's inequality, we obtain

$$\begin{aligned} \Pr(|\mathcal{N}_j^{\text{fr}} - \mu_j^{\text{fr}}| \leq \epsilon) &\geq 1 - \frac{(\sigma_j^{\text{fr}})^2}{\epsilon^2} = 1 - \frac{\langle n_j(t) \rangle}{\epsilon^2 c_0^2} \\ \Rightarrow \Pr(|\mathcal{N}_j^{\text{fr}} - \mu_j^{\text{fr}}| > \epsilon) &< \frac{\langle n_j(t) \rangle}{\epsilon^2 c_0^2}. \end{aligned} \quad (\text{C.3})$$

As the total number of particles in the bath goes to infinity ($c_0 \rightarrow \infty$), the average number of particles $\langle n_j(t) \rangle$ at any given shell will also go to infinity such that the ratio $\mu_j^{\text{fr}} = \langle n_j(t) \rangle / c_0$ is fixed. We know this ratio is finite because the equation satisfied by μ_j^{fr} is nothing more than a scaled version of Eq. (3.14). Nonetheless, the ratio $\langle n_j(t) \rangle / c_0^2$ will go to zero as $c_0 \rightarrow \infty$; therefore, this inequality implies $\mathcal{N}_j^{\text{fr}}$ will approach μ_j^{fr} in the large copy number limit, i.e. the law of large numbers. Consequently, $\mathcal{N}_j^{\text{fr}}$ will also approach the solution of Eq. (3.14) scaled by c_0 . Furthermore, we can carry the continuous limit for Eq. (3.14) scaled by c_0 , where the solution is $f^{\text{fr}}(r, t) = f(r, t)/c_0$. Consequently, the large particle number limit ($c_0 \rightarrow \infty$) of the ratio between local concentration and the bath state concentration satisfies the Smoluchowski equation with $f^{\text{fr}}(r_{\text{max}}, t) = 1$.

Note we could have normalized the random variable \mathcal{N}_j by any constant and obtain that $\int_{\sigma}^{r_{\text{max}}} f^{\text{fr}}(r, t) 4\pi r^2 dr \leq 1$, which means that $f^{\text{fr}} 4\pi r^2$ can be easily confused with a probability distribution function; however, it is not.